Journal of
Applied Remote Sensing

Actual evapotranspiration estimation for different land use and land cover in urban regions using Landsat 5 data

Wenjuan Liu
Yang Hong
Sadiq Ibrahim Khan
Mingbin Huang
Baxter Vieux
Semiha Caliskan
Trevor Grout

SPIE

Actual evapotranspiration estimation for different land use and land cover in urban regions using Landsat 5 data

Wenjuan Liu,[a,b] Yang Hong,[b] Sadiq Ibrahim Khan,[b] Mingbin Huang,[a,c] Baxter Vieux,[b] Semiha Caliskan,[d] and Trevor Grout[b]

[a] Northwest A&F University, College of Resource and Environment,
Yangling, Shaanxi Province, 712100, China
liuwenjuan66@gmail.com, hmbd@nwsuaf.edu.cn,

[b] University of Oklahoma, School of Civil Engineering and Environmental Science,
Center for Natural Hazard and Disaster Research, National Weather Center,
Norman, OK 73072
yanghong@ou.edu, sadiq@ou.edu, bvieux@ou.edu

[c] Institute of Soil and Water Conservation, Chinese Academy of Sciences and Ministry of Water Resources, Yangling, Shaanxi Province 712100, China

[d] University of Oklahoma, Department of Geography, Center for Spatial Analysis,
Norman, OK 73019
semihacaliskan@ou.edu

Abstract. Evapotranspiration (ET) is deemed critical for water resources management. Even in the same climatic and meteorological conditions, actual ET (ET_a) may exhibit remarkable spatial variability across different vegetation covers, agricultural land use practices, and differing types of urban land development. The main objectives of this study are (1) to evaluate the possible closure of the heat balance equation using Oklahoma's unique environmental monitoring network; and (2) to estimate ET_a and determine the variation with regards to varying types of land use and land cover in urban settings. In this study, a Surface-Energy-Balance ET algorithm was implemented to estimate ET_a at a higher spatial resolution using Landsat 5 satellite images while the Oklahoma Mesonet observations can be used as our ground truth data. Accuracy of the estimated ET_a was assessed using latent heat flux measurements provided by AmeriFlux towers. The associated bias ratios of daily mean ET_a with respect to both burn and control sites are -0.92%, and -8.86% with a correlation of 0.83 and 0.81, respectively. Additionally, estimated ET_a from a water balance budget analysis and the remotely sensed ET_a are cross-validated with a low bias ratio of 5.2%, and a correlation coefficient of 0.7 at the catchment scale. The lowest ET_a was observed for developed urban areas and highest for open water bodies. The ET_a difference is also demonstrated from two contrasting counties. The results show Garfield County (agricultural) has higher ET_a values than Oklahoma County (urban) for all land cover types except open water bodies.

Keywords: Evapotranspiration (ET); Landsat; Surface Energy Balance; land covers land use; urban development.

1 INTRODUCTION

Evapotranspiration (ET) is among the major components of the hydrologic cycle and is arguably the second most important (after precipitation) component of the water cycle for most of the global land area [1]. Therefore, for various disciplines, including hydrologic budgeting, water resource planning, agricultural irrigation, and ecological system risk

Received 2 Apr 2010; accepted 8 Nov 2010; published 19 Nov 2010 [CCC: 19313195/2010/$25.00]

management, quantification of spatial and temporal variability of ET is fundamentally important [2].

Typically, there are four methods for estimating ET: hydrological methods (water balance), direct measurement (e.g. lysimeters), micrometeorological methods (energy balance), and empirical or combination methods [3]. These methods are based on energy or climatic factors. Most of these methods can only provide point estimates of ET, which are not sufficient for large-scale assessment. Physics-based hydrologic models can compute ET patterns, but require enormous amounts of field data, which is often unavailable in many river basins across the world. During the last two decades, significant progress has been made in estimating actual ET (ET_a) using satellite remote sensing [4,7]. Remotely sensed data has the advantage of large area coverage, frequent updates, and consistent quality [8,10]. Remotely sensed data methods provide a powerful means to compute ET for individual pixels to the entire raster image.

The advantage of using Landsat imagery for ET estimations rests upon its high resolution of the visible and near infrared bands (Landsat-5) at 30 m spatial resolution and the thermal band (Landsat-7) at 60 m spatial resolution. Landsat 5 at 120 m spatial resolution can support field-scale ET estimation which is significant for water rights regulation and water resources planning [11]. Land use and land cover (LULC) can have significant but different control of soil moisture through the ET process [12]. In Southwestern Idaho, the ET difference was identified due to different types of LULC using field observations and remote sensing Landsat TM Data [13]. Spatiotemporal ET_a variations of different LULC in well developed urban areas turns out to be sensitive to a water cycle analysis in urban regions which has not been extensively studied before. The objectives of this study are: (1) to evaluate the possible closure of the heat balance equation using Oklahoma's unique environmental monitoring network; and (2) to estimate ET_a and determine the variation with regards to varying types of LULC in urban settings.

2 STUDY AREA, DATA AND METHODOLOGY

2.1 Study Area

The study area is a gauged watershed, located on the Skeleton Creek, in central Oklahoma, near Lovell, OK. This area covers approximately 1033.59km^2 and includes very diverse LULC from agriculture (Garfield County) to urban (Oklahoma County). The annual precipitation is around 870 (mm), and mean high and low temperatures are 21°C and 8 °C, respectively. The study area is in a semi-arid region where the agriculture activities were predominantly sustained by irrigation. Yet irrigated agriculture, rain-fed agriculture, wetlands, and riparian vegetation all evaporate and transport water into the atmosphere through the ET process.

The remotely sensed ET_a estimates were compared with calculated ET_a based on water balance over this basin. The locations and the land use classifications of the study area, and the basin are shown in the Fig. 1. Ground truth data sets were available through two sources. One is the Oklahoma Mesonet (http://www.mesonet.org) including eighteen Mesonet stations. The other is the AmeriFlux towers, which provide surface flux observations, established by the U.S. DOE's Atmospheric Radiation Measurement (ARM) Program in the Southern Great Plains (http://www.daac.ornl.gov/FLUXNET/fluxnet.html). In this study, two AmeriFlux towers were selected at the ARM SGP Burn site and ARM SGP Control site for comparative analysis.

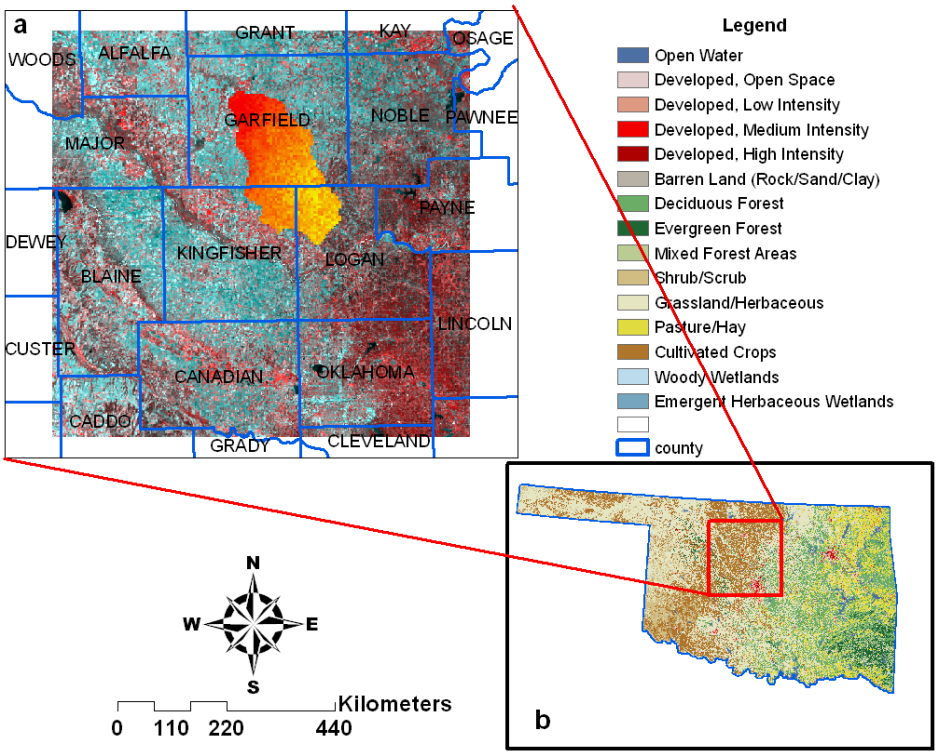

Fig. 1: (a) Landsat 5 (false color) of study area and (b) land use land cover map.

2.2 Data

2.2.1 Satellite Imagery

In this study, we used Landsat 5 which has a repeat cycle of 16 days and swath width of 185 km. Landsat 5 data (path 28; row 35) was extracted and processed from the Land Processes Distributed Active Archive Center (LP DAAC) at the USGS EROS Data Center, with the standard Hierarchical Data Format (http://LPDAAC.usgs.gov). The TM bands 1–5 and 7 provide reflectance data for the visible and near infrared radiation at 30m spatial resolution. TM band 6 measures thermal radiation, and, has a spatial resolution of 120m. ET cannot be calculated for cloud covered land surfaces, because even a thin layer of clouds can drop the thermal band readings considerably and cause large errors in calculation of sensible heat fluxes. It is crucial that images used in this research have clear skies.

2.2.2 Weather Data

Meteorological data was obtained from the Mesonet. The Mesonet, established in January 1994, measures a wealth of atmospheric and hydrologic variables including solar radiation, humidity, temperature, wind speed and direction, and soil moisture to aid in operational weather forecasting and environmental research across the state (http://www.mesonet.org). The observations of the Mesonet are made every 5 minutes.

2.2.3 Hydrologic Data

Precipitation data for 2005 was obtained from Mesonet. (http://www.mesonet.org). The

United States Geological Survey (USGS) has collected water-resources data at approximately 1.5 million sites across the United States, Puerto Rico, and Guam. Data provided by the USGS in Oklahoma including: stream discharge, water levels, precipitation, and components from water-quality monitors. Runoff data in 2005 over Skeleton creek was obtained from USGS water resources (http://www.usgs.gov).

2.3 Methodology

2.3.1 Surface Energy Balance Method

The theory of SEB is to estimate the ET as the residual of the energy balance equation:

$$LE = R_n - G - H \tag{1}$$

where LE is latent heat flux consumed by ET, R_n is net radiation (sum of all incoming and outgoing short-wave and long-wave radiation) at the surface, G is soil heat flux (sensible heat flux converted to the ground), and H is sensible heat flux to the atmosphere (units are Wm^{-2}). R_n, G, and H can be derived from satellite data and meteorological observations.

The R_n of SEB can be derived through remote sensing information and surface properties such as albedo, leaf area index, vegetation cover, surface temperature, and meteorological observations [2,14,15]. The equation to calculate the net radiation flux is given by

$$R_n = (1-\alpha)\cdot R_{swd} + \varepsilon \cdot R_{lwd} - \varepsilon \cdot \sigma \cdot T_s^4 \tag{2}$$

where α is the surface albedo, ε is the emissivity of the surface, R_{swd}, R_{lwd} are incoming shortwave and long wave radiation respectively, σ is the Stefan-Bolzmann constant, and T_s is the surface temperature.

The ground heat flux is estimated using surface temperature, albedo, and normalized difference vegetation index (NDVI).

$$G = R_n \cdot [(T_s - 275.15)\cdot (0.0038 + 0.0074\alpha)\cdot (1 - 0.98NDVI^4)] \tag{3}$$

The sensible heat flux is estimated as a function of the temperature gradient above the surface, surface roughness, and wind speed.

$$H = \rho_a \cdot Cp_a (T_{aero} - T_a)/r_{ah} \tag{4}$$

where ρ_a is air density (kg m^{-3}), C_{pa} is specific heat of dry air (1004 J kg^{-1} K^{-1}), T_a is average air temperature, (K), T_{aero} is average aerodynamic temperature (K), and r_{ah} is aerodynamic resistance (s m^{-1}) to heat transport.

2.3.2 Modified version of the surface energy balance approach

In this paper we utilized a modified version of the Surface Energy Balance (SSEB) approach to estimate ET_a. ET_a can be estimated by the near-surface temperature difference based on the land surface temperature (LST) of the hot and cold pixels in the study area. The cold pixels are selected as a wet, well irrigated crop surface having a full ground cover of vegetation, achieving maximum ET. On the contrary, the hot pixels are selected as a dry, bare agricultural field, where ET is assumed to be zero. The remaining pixels in the study area experience varying levels of ET proportional to their LST collectively defined by the hot and cold pixels [16]. Therefore, we need LST, Normalized Difference Vegetation Index (NDVI), and

reference ET in order to calculate actual ET. They are described as follows.

Land surface temperature: The instantaneous LST at pixel location (i, j) was extracted by using ERDAS IMAGINE 9.2 software package based on Eq. (5):

$$\mathrm{Ts}\ (\mathrm{i,j}) = \frac{\mathrm{K}_2}{\ln[\mathrm{k}_1/\mathrm{L}_6(i,j)+1]} \tag{5}$$

where, L_6 (i,j) is the uncorrected thermal radiance at pixel (i,j). K_1 and K_2 are calibration constants; the K_1 and K_2 constants for Landsat images are: K_1=607.8 and K_2=1261 for Landsat 5, and K_1=666.1 and K_2=1283 for Landsat 7. The units for K constants are W/m^2 /sr/ μ m.

The spectral radiance for each band is calculated using Eqs (6) and (7) given for Landsat 5 and 7. The spectral radiance for each band (L_λ), with unit W/m^2/sr/μm, is computed according to the Eq (6). This is the outgoing radiation energy of the band observed at the top of the atmosphere by the satellite.

$$\mathrm{L}_\lambda(i,j) = \frac{\mathrm{LMAX}-\mathrm{LMIN}}{\mathrm{QCALMAX}-\mathrm{QCALIMAX}} \times (\mathrm{DN(i,j)}-\mathrm{QCALMIN})+\mathrm{LMIN} \tag{6}$$

where DN is the digital number measured by satellite sensor at each pixel; LMAX and LMIN are calibration constants, QCALMAX and QCALMIN are the highest and lowest range of values for rescaled radiance in *DN*. For Landsat 5, QCALMAX = 255 and QCALMIN = 0, so Eq. (6) becomes:

$$\mathrm{L}_\lambda(i,j) = \frac{\mathrm{LMAX}-\mathrm{LMIN}}{255} \times \mathrm{DN(i,j)}+\mathrm{LMIN} \tag{7}$$

NDVI: The NDVI at pixel location (i, j) is calculated using the satellite reflectance of Band 3 and Band 4 of Landsat 5. It is computed using ERDAS IMAGINE 9.2 software package.

$$\mathrm{NDVI(i,j)} = \frac{\mathrm{RED(i,j)}-\mathrm{NIR(i,j)}}{\mathrm{RED(i,j)}+\mathrm{NIR(i,j)}} \tag{8}$$

where RED is reflectance in the red band and NIR is reflectance in the near infrared band.

Reference ET: The Oklahoma Mesonet reference ET (ET_r) model is based on the standardized Penman-Monteith reference evapotranspiration equation recommended by the American Society of Civil Engineers (ASCE) and the computational procedures found in [17,18]. The ASCE Standardized Reference ET equation [19] computes ET_r using Eq (9):

$$\mathrm{ET_r(i,j,t)} = \frac{0.408\Delta(\mathrm{R_n}-\mathrm{G})+\gamma\frac{\mathrm{C_n}}{\mathrm{T}+273}\mathrm{u_2}(\mathrm{e_s}-\mathrm{e_a})}{\Delta+\gamma(1+\mathrm{C_d}\mathrm{u_2})} \tag{9}$$

where ETr(i,j,t) is the standardized Reference ET at the (i,j) pixel that is calculated at hourly time step but usually expressed on a daily time scale (mm d^{-1}), R_n is the calculated net radiation at the crop surface (MJ m^{-2} d^{-1}for daily time steps), G is the soil heat flux density at the soil surface (MJ m^{-2} d^{-1}for daily time steps), T is the mean daily or hourly air temperature at 1.5 to 2.5 m height (°C), u_2 is the mean daily or hourly wind speed at 2 m height (m s^{-1}), e_s is the Saturation vapor pressure at 1.5 to 2.5 m height (kPa), for daily computation, the value is the average of e_s at maximum and minimum air temperature, e_a is the mean actual vapor pressure at 1.5 to 2.5 m height (kPa), Δ is the slope of the saturation vapor

pressure-temperature curve (kPa° C^{-1}), γ is psychrometric constant (kPa °C^{-1}), C_n = Numerator constant that changes with reference type and calculation time step, *Cd* = Denominator constant that changes with reference type and calculation time step. Note that for ground-based meteorological observations, we did not use the (i,j) location indicator since they are originally measured by Oklahoma Mesonet stations every 5 minutes.

ET Fraction (ET_f): With the assumption that hot pixels experience very little ET and cold pixels represent the maximum ET throughout the study area [16], the average temperature of hot and cold pixels could be used to calculate the proportional fractions of the ET on a per pixel basis. Thus, the ET fraction (ET_f) was calculated for each pixel by applying the Eq. (10) to Landsat 5 LST grids:

$$\mathrm{ET_f}(i,j,t) = \frac{\mathrm{T_{hot}} - \mathrm{T(i,j,t)}}{\mathrm{T_{hot}} - \mathrm{T_{cold}}} \tag{10}$$

where T_{hot} is the average temperature of the hot pixels selected for a given scene, T_{cold} is the average temperature of the cold pixels selected for that scene, and T(i,j,t) is the Landsat 5 LST value for the (i,j) pixel in the composite scene at the satellite overpass time t.

Actual ET (ET_a): Therefore, the ET_a at the (i, j) pixel can be estimated using Eqs (11):

$$\mathrm{ET_a}(i,j,t) = \mathrm{ET_f}(i,j,t) \times \mathrm{ET_r}(i,j,t) \tag{11}$$

A key assumption of this method is that the ET_f is almost constant for a given day, which is frequently confirmed to be the case [20,23]. This allows an instantaneous estimate of ET_f at Landsat 5 overpass times to be extrapolated to estimate the daily actual ET.

Daily Actual ET ($ET_{a\ daily}$): Finally, the daily actual ET can thus be determined by:

$$\mathrm{ET_{a\,daily}}(i,j) = \sum_{t=1}^{day=24\,h} (\mathrm{ET_f}(i,j) \times \mathrm{ET_r}\,(i,j,t)) \tag{12}$$

where, $ET_{a\ daily}$ is the actual ET on a daily basis (mm d^{-1}), t is the hourly temporal resolution of computed reference ET using the Eqs (9) from the Oklahoma Mesonet station observations.

3 RESULTS AND DISCUSSION

3.1 AmeriFlux Tower Based Evaluation

In this study, the comparison between SEB-ET and American flux ET was conducted primarily at a daily time scale. The ARM SGP Burn site is located in the native tall grass prairies of the USDA Grazinglands Research Laboratory near El Reno, Canadian County. One of two adjacent 35ha plots, the US-ARb plot was burned on March 8th 2005. The second plot, US-ARc, was left unburned as the control for experimental purposes. Aside from 2005, the region evaded burning activities for at least 15 years. Current disturbances consist of only light grazing activities. Table 1 shows a summary of statistics for 2005 daily ET comparison. In Table 1, the Root Mean Square Errors (RMSE), bias ratio, and Correlation Coefficients (CC) are presented on a daily basis. In general, bias ratios are less than 10% of the mean values on a daily basis with a correlation of 0.83 for burn areas, and 0.81 for control areas. The lowest bias is -0.92%, observed at the burn site. The SEB accuracy assessment shows relatively high RMSE of 0.95 mm and 0.99 mm. The best way to explain this is that we used Landsat images with a relatively coarse temporal resolution (e.g. 16-day return visit) to

compute the ET fraction. It is assumed that the ET fraction, calculated at the satellite overpasing time, can be extrapolated for the 16-day time period. Therefore, daily time series validation using the SEB method with ET fraction, having a coarse temporal resolution, likely decreases the daily correlation coefficients and RMSE.

SEB-ET values and AmeriFlux ET measurement have strong linear correlations at both sites. It presents a good association between SEB-based ET and AmeriFlux ET. From Fig. 2, we can see the largest difference occurs during the winter months (between day 1 and day 100). The AmeriFlux ET measurements show fewer fluctuations, while the SEB-ET shows many more fluctuations. In addition to these differences, the SEB-ET values are generally higher than the AmeriFlux ET measurements.

Table 1. Comparisons of SEB-based ET_a estimates and observed values collected at AmeriFlux site in 2005.

Site	Time	AmeriFlux mean (mm)	SEB mean (mm)	Bias ratio (%)	RMSE (mm)	CC
Burn	Daily	2.00	1.95	-0.92	0.95	0.81
Control	Daily	2.21	1.98	-8.68	0.99	0.83

*Bias ratio = (estimates-observations)/observations x100%
*RMSE = Root Mean Square Error
*CC= Correlation Coefficient

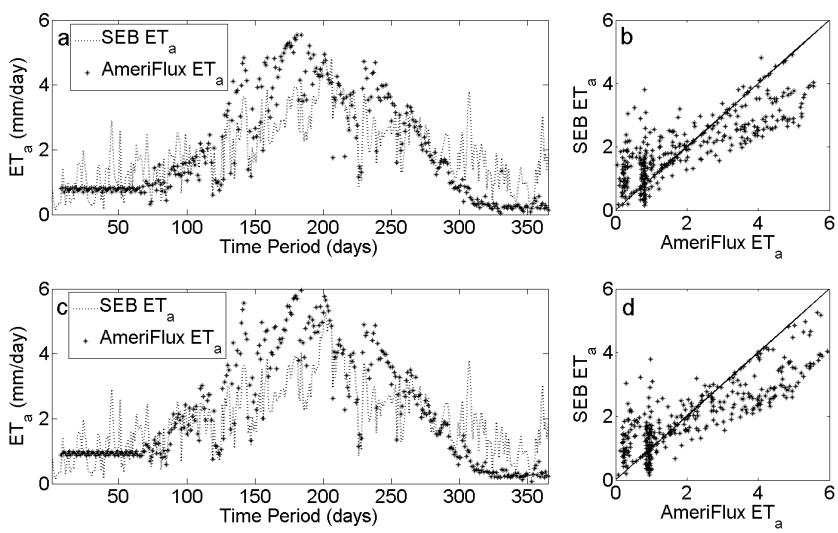

Fig. 2. Comparisons of daily ET_a between AmeriFlux tower observations and the remote sensing-based ET_a estimates in 2005. Panel (a) daily time series at Burn site and (b) scatter plot for burn site. Panel (c) daily time series at control site and (d) scatter plot for control site.

3.2 Basin-Based Evaluation

The SEB-ET is also cross-validated with the water balance budgeted ET in the basin. The water budget method used the data as shown in Table 2 and follows Eq. (10):

$$\Delta S = P - R - ET_a \tag{13}$$

where ΔS is the change in storage, P is precipitation, R is runoff, and ET_a is actual ET. This water budget assumes that there is no significant change in storage from year to year (ΔS=0), which allows for computing the ET_a.

Table 2 shows several hydro-meteorological parameters that were used to calculate the water budget. When the change in storage becomes relatively insignificant, ET_a can be assumed equal to the difference between precipitation and run-off [24]. Table 3 shows monthly values comparisons between the SEB-ET estimates and the ET estimates based on the water balance budget. By using monthly values, it shows that the bias ratio is 5.2% with a correlation coefficient of 0.7 at the catchment scale. The SEB-ET monthly mean is 64.34 mm and the monthly mean ET value based on water balance budget method is 61.16 mm.

Table 2. Data for basin used for the water balance.

Component	Location	Data Source	Period
Precipitation	Marshall, Oklahoma	Mesonet	Jan.2005-Dec.2005
Direct Runoff	Skeleton Creek Runoff gauge #07160500	USGS	Jan.2005-Dec.2005

Table 3. Comparisons of the ET estimates based on Landsat 5 and water balance budget analysis associated with 2005 monthly average in the basin.

Time scale	Rainfall mean (mm)	Runoff mean (mm)	SEB-ET mean (mm)	Water Balance ET (mm)	Bias ratio (%)	CC
Monthly	73.36	12.35	64.34	61.16	5.20	0.70

*Bias ratio = (estimates-observations)/observations x100%
*CC= Correlation Coefficient

3.3 Spatial Variability Analysis of the ET

Figure 3(a) shows the spatial variations of ET-SEB estimates based on Landsat 5 data in the study area on July 31st 2005. The daily ET_a shows significant spatial variations, ranging from less than 1mm in developed areas to 7.53mm in water-bodies such as lakes or rivers, with the daily mean ET_a of 3.28mm for the whole study area. Figure 3(b) displays the spatial variations of the ET_a for two distinctly different types of LULC. The results indicate ET_a for irrigated agriculture and water bodies is high, while for urban areas ET_a is low. This indicates that ET_a is controlled by types of LULC and water availability at the same time. Seasonal and annual ET_a can vary over different types of LULC such as agricultural fields, rivers, lakes, and build-up areas at the field scale or high-resolution grid scale. SEB-ET_a estimates for the study area in 2005 (Figure 4) are based on Landsat 5 data. The mean ET_a is 776.16mm and the spatial variations of ET_a ranges from 92 to 1,337mm.

4 RELATIONSHIP BETWEEN ETA AND LAND USE/LAND COVER TYPES AND URBAN DEVELOPMENTS

In order to examine the ET_a for different types of LULC, seven types of LULC were selected in the study area including agriculture lands (different types of crop, irrigated land, and dry land), water bodies (lakes, rivers, etc.), forests (deciduous forest, evergreen forest, and mixed forest), grass land, wetlands (woody wetlands), urban areas (having development levels of open-land, low intensity, medium intensity, high intensity), and shrub lands.

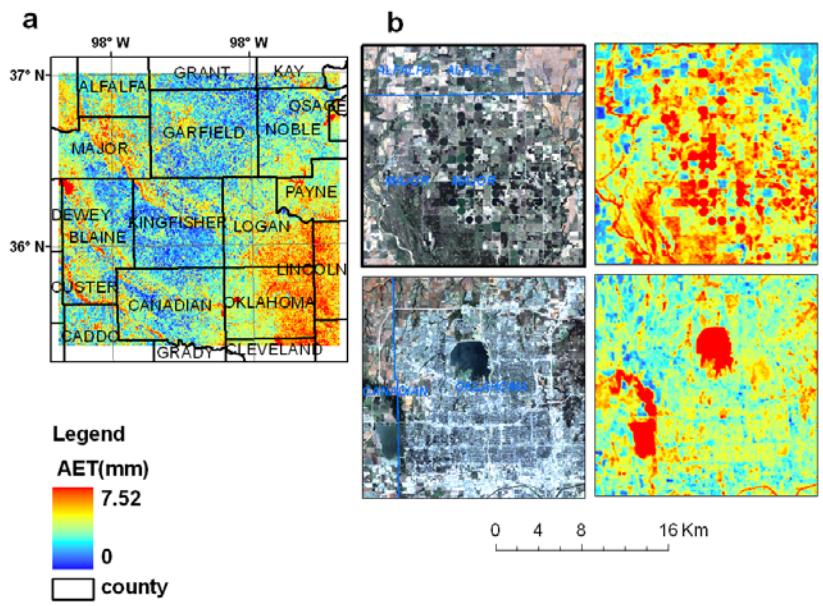

Fig. 3. (a) Spatial variations of the ET_a (mm) over the study area in 2005. (b) upper left side is Landsat false color image. Fig 3 (b) located right side shows local spatial variations of the ET_a (mm) at agricultural areas and Fig 3 (b) located at lower right side shows local spatial variations of the ET_a (mm) at urban areas nearby a water body on July 31th 2005. Note: AET stands for the actual ET.

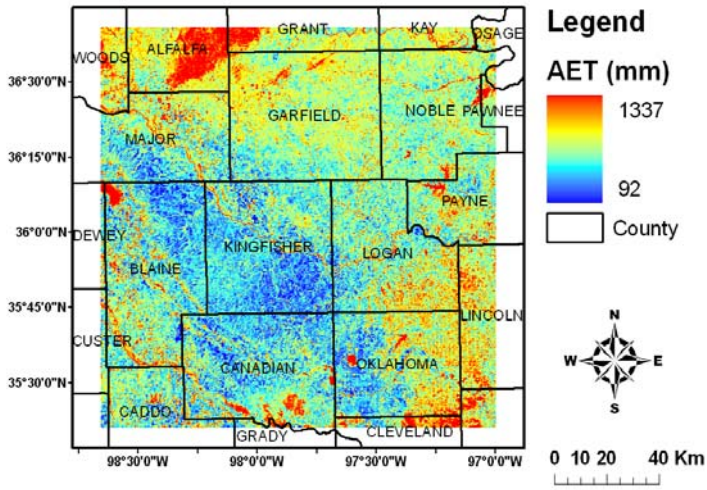

Fig. 4. Spatial variations of the ET_a (mm) in the study area, 2005. Note that AET stands for the actual ET.

4.1 The Annual ET_a in the Whole Study Area

Statistics were extracted by overlaying the LULC map of the whole study area. The results of the annual mean ET_a values are shown in Table 3 corresponding to the seven types of LULC. The top three values of the ET_a associated with designated types of LULC include water bodies, wetlands, and forests, and all ET_a values are over 800 mm year^{-1}. The results clearly indicate that the ET_a values in the agriculturally dominant Garfield County are generally higher than those in Oklahoma County except for water bodies. Also, Fig. 3(b) shows the ET_a values for irrigated crop lands are high during growing season, but the annual ET_a values for agriculture are not necessarily higher than those for grass and shrub lands as listed in Table 3. This could be mainly due to the fact that the ET values for the non-irrigated crop lands during non-growing seasons are lower than those at the other two vegetated lands. The developed areas generally have the lower ET values because of the lower soil moisture availability [25]. Thus, the energy transformation is mainly limited in the form of sensible heat exchange.

Table 3. Annual ET by land use/land cover class over the study area, Garfield county (agricultural) and Oklahoma county (urban) during 2005.

Types of LULC	The whole area (mm)	Garfield (mm)	Oklahoma (mm)
grass	774.26	804.12	763.89
developed area	717.18	767.83	708.69
open water	1019.37	919.27	990.28
forest	854.24	858.76	831.59
wetland	897.90	870.77	835.89
agriculture	778.18	796.51	732.18
shrubland	769.95	807.41	743.31

4.2 The Monthly Actual ET in the Whole Study Areas

Figure 5 shows the monthly ET_a variations for the selected eight types of LULC for the study area. In general, all types of LULC show similar seasonal dynamic trends for ET_a throughout the year. The value of ET_a started to rise rapidly in April, reached peak values in July, and then declined to the lowest levels in January in 2005. The results also show that water bodies have the highest ET_a values over the whole year (See Fig. 5). Wetlands and forests have higher average ET_a than agriculture land, and grass land. Similar to the annual analysis, the lowest ET values occur at the developed areas throughout the year.

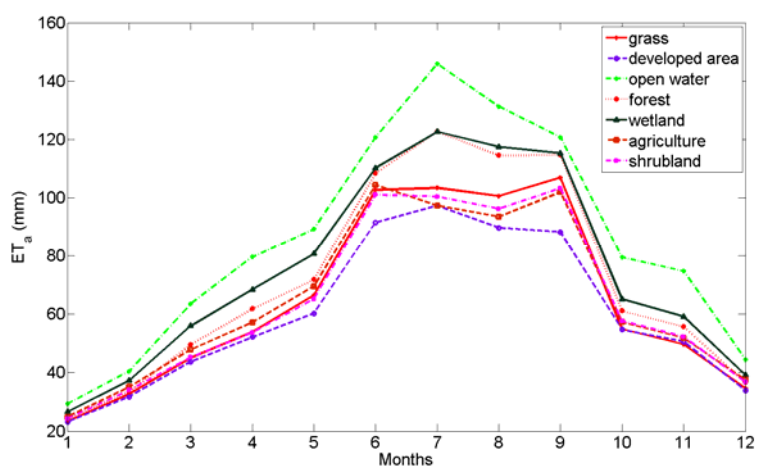

Fig. 5. Monthly ET by land use/land cover types in the study area.

4.3 Actual ET for Different Urban Development Levels

The monthly ET_a for different types of urban areas as defined in Table 4 was estimated for Oklahoma City. Figure 6(a) presents the seasonal ET_a variations for the four different types of urban areas. In general, all types of urban areas show similar ET trends throughout the year. The values of ET_a started to rise rapidly in May, reached peak values in July, and then declined for the rest of the year. The results also show that open land areas have the highest ET_a values during the whole year (Fig. 6b). The lower the urban development level, the higher the annual ET_a values. Figure 6(a) also indicates that the relative differences of the ET_a occur in association with urban development levels from April to September, whereas the difference is negligible in fall and winter seasons.

Table 4. Description of development levels in urban regions based on National Land Cover Data (NLCD).

Urban development levels	Descriptions
Open Space	Includes areas with a mixture of some constructed land, but mostly vegetation cover in the form of lawn grasses. Impervious surfaces account for less than 20 percent of total cover. These areas most commonly include large-lot single-family housing units, parks, golf courses, and vegetation planted in developed settings for recreation, erosion control, or aesthetic purposes.
Low Intensity	Includes areas with a mixture of constructed land and vegetation cover. Impervious surfaces account for 20–49 percent of total cover. These areas most commonly include single-family housing units.
Medium Intensity	Includes areas with a mixture of constructed land and vegetation cover. Impervious surfaces account for 50–79 percent of the total cover. These areas most commonly include single-family housing units.
High Intensity	Includes highly developed areas where people reside or work in high numbers. Examples include apartment complexes, row houses, and commercial/industrial. Impervious surfaces account for 80 to 100 percent of the total cover.

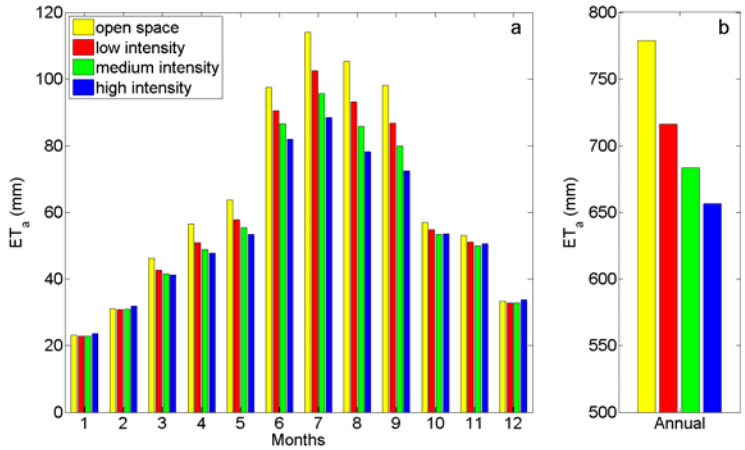

Fig. 6. (a) Monthly ET by different developed intensity in Oklahoma county during 2005. (b) Annual ET by different developed intensity in Oklahoma county during 2005.

5 CONCLUSIONS

This study presents the estimates of remotely sensed ET_a using Surface Energy Balance method and examines the spatiotemporal variations of ET_a in terms of four types of LULC in urban region in Oklahoma. Landsat 5 data and Oklahoma Mesonet data were used to support estimating actual ET values. Major findings include: 1) The accuracy of remotely sensed ET results was validated by using site-specific flux towers and a water balance model at the basin scale. Results show that SEB algorithms can be used to effectively estimate ET at the regional level. 2) Different types of LULC significantly reflect different ET_a in urban regions. Overall, water bodies have the highest ET, wetlands and forests present a higher rate of ET than grass and agricultural lands, and the highly developed areas have the lowest ET. With seasonal water-use quantified for different types of land cover those estimates of ET_a could help create managerial strategies to improve water management. 3) The estimates ET_a reveal that the higher the ET the lower development levels in urban regions.

However, ET calculated through SEB potentially has systematical errors. The sources of the error including inherent calibration bias of Landsat land surface temperature data, assumption of the sub-daily consistent ET Fraction and reference ET model. With a single thermal band, obtaining the LST from Landsat data is very difficult, and might cause systematic errors. Consequently, the LST derived from Landsat data might have bias due to different emissivity of infrared radiation. In addition, the ground truth observations might also have some measurement errors. Nevertheless, the estimation of ET using a high-resolution satellite remote sensing technology in urban regions can be still deemed as promising. Such a method complements the conventional procedures that solely rely on land surface point-based ET estimation approaches.

Acknowledgments

This work was financed by the United State Geological Survey and the Oklahoma Water Resources Research Institute. Partial funding for the first author was also provided by the State Scholar Council, Ministry of Education of China. The authors would like to extend their appreciation to Oklahoma MESONET for meteorological data. The authors are also thankful

to Professor Margaret Torn, Lawrence Berkeley National Laboratory Earth Science Division, Berkeley, CA, for providing the quality-controlled AmeriFlux tower observations.

References

[1] R. Allen, L. Pereira, D. Raes, and M. Smith, "Crop evapotranspiration -guidelines for computing crop water requirements-FAO Irrigation and drainage paper 56," *FAO, Rome*, **300** (1998).

[2] R. Allen, M. Tasumi, and R. Trezza , "Satellite-based energy balance for mapping evapotranspiration with internalized calibration (METRIC)—model," *J. Irrig. Drain. Eng.* **133**, 380 (2007) [doi:10.1061/(ASCE)0733-9437(2007)133:4(380)].

[3] C.W. Thomthwaite and J. R. Mather The water balance Publications in climatology Centerton NJ:Drexel Institute of Technology **8** (1955)

[4] W. G. M. Bastiaanssen, "SEBAL-based sensible and latent heat fluxes in the irrigated Gediz Basin, Turkey," *J. Hydrol*. **229**(1-2), 87-100 (2000) [doi:10.1016/S0022-1694(99)00202-4].

[5] W. G. M. Bastiaanssen, M. Menenti, R. A. Feddes, and A. A. M. Holtslag, "A remote sensing surface energy balance algorithm for land (SEBAL). 1. Formulation," *J. Hydrol*. **212**, 198-212 (1998) [doi:10.1016/S0022-1694(98)00253-4].

[6] W. P. Kustas, G. R. Diak, and M. S. Moran, "Evapotranspiration, Remote Sensing of." *Encyclopedia of Water Science*, Dekker, New York (2003) [doi: 10.1081/E-EWS-120010313].

[7] W. P. Kustas and J. M. Norman, "Use of remote sensing for evapotranspiration monitoring over land surfaces," *Hydrol. Sci. J.* **41**(4), 495-516 (1996) [doi:10.1080/02626669609491522].

[8] Q. Mu, F. A. Heinsch, M. Zhao, and S. W. Running, "Development of a global evapotranspiration algorithm based on MODIS and global meteorology data," *Remote Sens. Environ*. **111**(4), 519-536 (2007) [doi:10.1016/j.rse.2007.04.015].

[9] J. A. Sobrino, M. Gomez, J. C. Jimenez-Munoz, and A. Olioso, "Application of a simple algorithm to estimate daily evapotranspiration from NOAA-AVHRR images for the Iberian Peninsula," *Remote Sens. Environ.* **110**(2), 139-148 (2007) [doi:10.1016/j.rse.2007.02.017].

[10] K. Wang, P. Wang, Z. Li, M. Cribb, and M. Sparrow, "A simple method to estimate actual evapotranspiration from a combination of net radiation, vegetation index, and temperature," *J. Geophys. Res*. **112**, D15107 (2007) [doi:10.1029/2006JD008351].

[11] R. G. Allen, M. Tasumi, A. Morse, and R. Trezza , "A Landsat-based energy balance and evapotranspiration model in Western US water rights regulation and planning," *Irrig. Drain. Sys.* **19** (3), 251-268 (2005) [doi:10.1007/s10795-005-5187-z].

[12] Y. K. Zhang and K. E. Schilling, "Effects of land cover on water table, soil moisture, evapotranspiration, and groundwater recharge: a field observation and analysis," *J. Hydrol*. **319** (1-4), 328-338 (2006) [doi:10.1016/j.jhydrol.2005.06.044].

[13] A. Morse, W. J. Kramber, and R. G. Allen, "Preliminary computation of evapotranspiration by land cover type using Landsat TM data and SEBAL," *IEEE Int. Geosci. Remote Sens. Symp.* **4**, 2956-2958 (2003) [doi: 10.1109/IGARSS.2003.1294644].

[14] Z. Su, "The Surface Energy Balance System(SEBS) for estimation of turbulent heat fluxes," *Hydrol. Earth Syst. Sci*. **6** (1), 85-99 (2002) [doi:10.5194/hess-6-85-2002].

[15] W. G. M. Bastiaanssen, E. J. M. Noordman, H. Pelgrum, G. Davids, B. P. Thoreson, and R. G. Allen, "SEBAL model with remotely sensed data to improve water-resources management under actual field conditions," *J. Irrig. Drain. Eng.* **131**, 85 (2005) [doi:10.1061/(ASCE)0733-9437(2005)131:1(85)].

[16] G. B. Senay, M. Budde, J. P. Verdin, and A. M. Melesse, "A coupled remote sensing and simplified surface energy balance approach to estimate actual evapotranspiration from irrigated fields," *Sensors* **7**(6), 979-1000 (2007) [doi:10.3390/s7060979].

[17] R. Allen, M. Smith, L. Pereira, and A. Perrier, "An update for the calculation of reference evapotranspiration," *ICID Bull.* **43** (2), 35-92 (1994).

[18] R. Allen, M. Smith, A. Perrier, and L. Pereira, "An update for the definition of reference evapotranspiration," *ICID Bull.* **43** (2), 1-34 (1994).

[19] M. Jensen, R. Burman, and R. Allen, "Evapotranspiration and irrigation water requirements," *Proc. ASCE* **70** (1990).

[20] W. Brutsaert and M. Sugita, "Application of self-preservation in the diurnal evolution of the surface energy budget to determine daily evaporation," *J. Geophys. Res*. **97**(18), 377–318 (1992).

[21] W. J. Shuttleworth, R. J. Gurney, A. Y. Hsu, and J. P. Ormsby, "FIFE: the variation in energy partition at surface flux sites," *IAHS Publ*. **186**, 67–74 (1989).

[22] M. Sugita and W. Brutsaert, "Daily evaporation over a region from lower boundary layer profiles measured with radiosondes," *Water Resour. Res*. **27**(5), 747–752 (1991) [doi:10.1029/90WR02706].

[23] R. D. Crago, "Comparison of the evaporative fraction and the Priestley-Taylor alpha for parameterizing daytime evaporation," *Water Resour. Res.* **32**(5), 1403-1409 (1996) [doi:10.1029/96WR00269].

[24] F. I. Morton, "Operational estimates of areal evapotranspiration and their significance to the science and practice of hydrology," *J. Hydrol (Amsterdam)*, **66** (1/4), 1-76 (1983) [doi:10.1016/0022-1694(83)90177-4].

[25] F. Li, T. J. Jackson, W. P. Kustas, T. J. Schmugge, A. N. French, M. H. Cosh and R. Bindlish, "Deriving land surface temperature from Landsat 5 and 7 during SMEX02/SMACEX," *Remote Sens. Environ.* **92** (4), 521-534 (2004) [doi:10.1016/j.rse.2004.02.018].